INTERNATIONAL JOURNAL OF HYDROGEN ENERGY 41 (2016) 6457–6468

Available online at www.sciencedirect.com

ScienceDirect

journal homepage: www.elsevier.com/locate/he

Synthesis and performance of palladium-based electrocatalysts in alkaline direct ethanol fuel cell

L.P.R. Moraes [a,*], B.R. Matos [b], C. Radtke [c], E.I. Santiago [b], F.C. Fonseca [b], S.C. Amico [a], C.F. Malfatti [a]

[a] LAPEC/PPGE3M, Universidade Federal do Rio Grande do Sul, Avenida Bento Gonçalves, 9500, 91501-970, Porto Alegre, RS, Brazil

[b] Instituto de Pesquisas Energéticas e Nucleares, IPEN-CNEN, Avenida Prof. Lineu Prestes, 2242, São Paulo, SP, 05508000, Brazil

[c] Instituto de Química, Universidade Federal do Rio Grande do Sul, Avenida Bento Gonçalves, 9500, 91501-970, Porto Alegre, RS, Brazil

ARTICLE INFO

Article history:
Received 20 October 2015
Received in revised form
23 February 2016
Accepted 23 February 2016
Available online 28 March 2016

Keywords:
Alkaline direct ethanol fuel cell
Ethanol electrooxidation
Electrocatalysts
Carbon support

ABSTRACT

The present study reports the performance enhancement of alkaline direct ethanol fuel cell (ADEFC) by using non-functionalized (Vulcan) and functionalized (Vulcan-F) carbon supported Pd, PdSn, PdNi and PdNiSn anodic electrocatalysts produced by impregnation-reduction method. The electrocatalysts are studied by thermogravimetric analysis (TGA), X-ray diffraction (XRD), transmission electron microscopy (TEM), cyclic voltammetry (CV), and ADEFC stability tests. TGA measurements of Vulcan evidence the characteristic weight losses attributed to the presence of surface functional groups due to the acid treatment. XRD shows that a higher degree of alloying is reached between Pd and Sn, whereas the Ni in PdNi and PdNiSn exists mostly segregated in the oxide form. TEM analysis indicates an agglomeration of Pd and PdSn particles, whereas a more uniform particle distribution is observed for PdNi and PdNiSn samples. CV curves show that the onset potential is shifted towards negative values for binary and ternary samples supported on functionalized Vulcan (Vulcan-F) indicating that the ethanol oxidation is facilitated on the functionalized surface. ADEFC fuel cell tests reveal that the highest open circuit voltage and maximum power density are achieved for the PdNiSn supported on Vulcan-F in which the characterizations evidenced improved textural properties.

Copyright © 2016, Hydrogen Energy Publications, LLC. Published by Elsevier Ltd. All rights reserved.

Introduction

Recently, alkaline direct ethanol fuel cells (ADEFC) have attracted considerable attention due to technical and technological advantages over acid direct ethanol fuel cells, which have positioned them as a promising alternative for obtaining a more efficient ethanol conversion and a higher power density output [1]. One of the main advantages of ADEFC is the opportunity for developing new platinum-free electrocatalysts for the ethanol oxidation (EOR) and oxygen reduction

* *Corresponding author*. Tel./fax: +55 51 33089406.
E-mail address: leticia.moraes@ufrgs.br (L.P.R. Moraes).

http://dx.doi.org/10.1016/j.ijhydene.2016.02.150

0360-3199/Copyright © 2016, Hydrogen Energy Publications, LLC. Published by Elsevier Ltd. All rights reserved.

(ORR) reactions [1]. Such achievement could dramatically reduce the cost of the electrodes boosting this technology towards commercialization.

In opposition to acid direct ethanol fuel cells (DEFC), the electric transport of hydroxyl ions (OH^-) occurs from the cathode to the anode, i.e., against the ethanol flow through the electrolyte. The counterflow of charges in the electrolyte reduces the ethanol crossover due to the electroosmotic drag and results in a significant increase of the open circuit potential (~200 mV) [1,2]. Previous results showed that palladium (Pd) has a higher catalytic activity, higher CO tolerance, and better steady-state performance for ethanol electrooxidation than platinum (Pt) in alkaline media [1,3]. Moreover, the abundance of adsorbed hydroxyl groups (OH) at the catalyst surface plays an important role in both reducing the poisoning effect of carbonyl species and accelerating the anodic reactions towards a more efficient 12-electrons oxidation of ethanol [4,5].

However, the main disadvantage of ADEFC is the absence of an electrocatalyst that can trigger the complete oxidation of ethanol at a high rate. The challenges involved in electrooxidation of ethanol are: i) the pronounced increase of the number of adsorbed intermediates, such as acetaldehyde, acetic acid and carbon monoxide; and ii) the high energy required for the C–C bond breaking [2,6]. Therefore, Pd-based electrocatalysts have great potential to replace Pt at the anode due to its higher catalytic properties in alkaline media and to the lower cost [1,5–7]. However, unary Pd catalysts display disadvantages similar to Pt, such as the loss of stability that reduces the long-term ADEFC performance [8]. The Pd stability loss was mainly associated with changes of both the morphology and the size distribution of catalyst nanoparticles during fuel cell operation. Nevertheless, such parameters can be controlled by the addition of a cocatalyst or by the preparation of catalysts with different morphologies [8]. Previous chronoamperometry (CA) studies reported enhanced stability of binary catalyst such as PdNi, PdRh, and PdCo, which was possibly related to reduced poisoning of Pd [9–11]. Nonetheless, fuel cell stability evaluation using the Pd-based catalysts is rarely found [12].

The electrochemical performance of PdNi/C and PdSn/C for the ethanol electrooxidation in alkaline media have been studied by cyclic voltammetry as well as the ADEFC tests [2,3,13–15]. The results evidenced that the onset potential for ethanol oxidation of both PdNi/C and PdSn/C electrodes shifted negatively compared with that of Pd/C indicating a higher catalytic activity for these binary electrodes [3,13]. However, the higher performance of such compounds was attributed to different mechanisms. For PdNi/C, the higher performance was attributed to the presence of hydrous oxide surfaces, which is a donor of the oxygen-containing species to promote the CO to CO_2 oxidation, releasing the active sites on noble metal for further electrochemical reaction [3]. For PdSn/C, the higher catalytic activity was assigned to the high degree of Pd–Sn alloying, which changes the electronic structure of Pd, thereby reducing the activation barrier of the EOR [13]. Recent studies have shown that the surface functionalization of the carbon support in acid media can increase the number of oxygenated species at the surface and remove sulfur contaminants, thereby improving the catalytic properties of Pd-based electrocatalysts [24]. However, the effect of functionalization of the catalyst support for the development of new electrocatalysts was poorly explored.

The enhanced electrocatalytic properties of binary catalysts was reflected on the performance of ADEFC anodes impregnated with PdNi/C and PdSn/C [2,14,15]. The ADEFC tests using PdNi/C exhibited higher maximum power density (p_{max}) ~ 30 mW cm^{-2} with respect to Pd/C (~20 mW cm^{-2}) [14]. Similarly, other authors found that using PdNi/C p_{max} is ~45 mW cm^{-2}, whereas for Pd/C p_{max} was ~35 mW cm^{-2} [2]. The use of PdSn/C alloys with low Sn content in the ADEFC anode resulted in p_{max} values of ~16 mW cm^{-2} [15]. It is worth noting that the development of electrocatalysts for ethanol oxidation in alkaline media has been concentrated in the synthesis and characterization of bi-metallic alloys and the study of ternary electrocatalysts for ADEFC is incipient. Although extensive research efforts have been dedicated to the study of the physicochemical and electrochemical properties of the electrocatalysts, few studies are devoted to evaluate the performance of these materials in ADEFC measurements. Moreover, a systematic comparison between different electrocatalysts such as Pd/C, PdNi/C and PdSn/C in ADEFC tests using the same operational conditions is rarely found. It is well known that the maximum power density values obtained in ADEFC are dependent on several parameters such as the electrolyte membrane used, the operating temperature, the flow rate and concentration of the fuel solution [1,16,17]. The fuel cell response is usually evaluated by comparing the performance of the developed catalyst of a single type, such as PdSn or PdNi, to that of Pd/C [1,2]. The comparison between binary and ternary catalysts using the same operating fuel cell station is crucial for evaluating the advancement of the novel electrocatalysts with respect to the state-of-the-art Pd.

In this study, Pd, PdNi, PdSn, and PdNiSn electrocatalysts are synthesized on surface functionalized Vulcan by the impregnation-reduction method. A higher catalytic performance was observed in the electrochemical measurements of Pd and PdSn. However, PdNiSn exhibited a higher ADEFC performance for ethanol oxidation reaction in alkaline medium, which was associated with microstructural properties such as particle size and distribution.

Experimental

Catalyst preparation

The carbon-supported Pd-based electrocatalysts, represented by Pd/C, PdSn/C, PdNi/C and PdNiSn/C, were synthesized by the impregnation/reduction method. The catalyst synthesis consisted of impregnating on the high surface area carbon (Vulcan XC72R) with an ethylene glycol solution (75:25 v/v) containing the respective precursors $PdCl_2$, $NiCl_2$ and $SnCl_2$, under sonication for 30 min. The pH of the solution was adjusted in the basic range (pH ~ 12) and the suspension was kept for 3 h at 130 °C in reflux under stirring for reducing the ion metal precursors. The impregnated carbon was then washed and dried in a resistive furnace at 80 °C. The electrocatalysts PdSn/C, PdNi/C and PdNiSn/C with nominal

percentage compositions of 86:14, 60:40 and 40:50:10 were prepared. The same set of electrocatalysts was prepared using surface functionalized carbon, represented by Pd/C_F, $PdSn/C_F$, $PdNi/C_F$ and $PdNiSn/C_F$. The functionalization consisted of dispersing 1 g of carbon (Vulcan XC-72R) in a 2 mol L^{-1} solution of nitric acid (HNO_3) for 5 min under ultrasonic bath. This mixture was refluxed under stirring at 80 °C for 24 h and copiously washed with deionized water and dried in an oven at 80 °C.

Characterization

The catalyst composition was evaluated by Energy Dispersive X-ray (EDX), using a scanning electron microscope (Philips XL30) equipped with a microanalyzer EDAX DX-4 with an electron beam of 20 keV. Rutherford backscattering spectroscopy (RBS) measurements were performed to confirm the catalyst composition. The RBS analyses were performed using a He^+ beam at 2 MeV produced by TANDEM accelerator of 3 MV. In all the cases, the incidence beam was perpendicular to the sample surface and the detection angle was 165° related to beam direction. Both EDX and RBS measurements were performed in triplicate using different samples. The presented results correspond to the average value of three measurements. Thermogravimetric Analyses (TGA) were carried out in Setaram LabSys with a heating rate 10 °C min^{-1}, synthetic air flow of 25 mL min^{-1} in the 25–900 °C *T*-range. The average crystallite size was estimated from X-ray diffraction (XRD, Rigaku-Multiflex), and measurements were carried out in the 2θ range 20–90° and using Cu Kα radiation. The average crystallite size was estimated using the (220) peak of the Pd diffraction patterns by using Scherrer's Equation [20]. Transmission electron microscopy (TEM) measurements were performed on JEOL-2100F with applied 200 kV and the histograms of the particle size distribution were built by sampling 300 nanoparticles in an arbitrarily chosen area. Electrochemical experiments were carried out with a three-electrode cell and Autolab PGSTAT 302N potentiostat. A platinum wire and saturated calomel electrodes (SCE) were used as counter and reference electrodes, respectively, whereas a glassy carbon with an area of 0.196 cm^2 was used as working electrode. Cyclic voltammetry measurements of the electrocatalysts were performed in a 1.0 mol L^{-1} NaOH solution with 50 mV s^{-1} scan rate in the −0.8 to 0.3 V (versus saturated calomel electrode - SCE). The electrochemical surface active area was estimated from the calculation of the oxide reduction peak area assuming a charge of 405 μC cm^{-2} according with previous reports [19]. The current density values were normalized by the active surface area [19]. Stabilization tests were performed by CV curves recording 200 cycles sweeping between −0.8 V–0.3 V at scan rate of 50 mV s^{-1}.

ADEFC tests

The intermediate-temperature (*T* ~ 100 °C) ADEFC tests were conducted using sodium hydroxide embedded Nafion membranes as electrolyte. Nafion membranes (N117, DuPont) underwent the standard procedure for cleaning and protonic activation [21,22] with successive washing steps immersing the membranes in NaOH (6 mol L^{-1}) e H_2O_2 (3 vol%) at 80 °C for 1 h, with intermediate washing steps with deionized water (>15 MΩ, Millipore). The anode was prepared with synthesized catalysts and Nafion loadings of 1.0 mg cm^{-2} and 30 wt%, respectively. The cathode is composed of Pt/C (Pt/C E-TEK, 20% of Pt) and Nafion loadings of 1.0 mg cm^{-2} and 30 wt%, respectively. Both electrocatalyts were quantitatively deposited onto gas diffusion layers, composed by 35 wt% PTFE-treated carbon cloth, to form the gas diffusion electrodes as described elsewhere [21]. The membrane-electrode assemblies (MEAs) were fabricated by hot pressing the anode and the cathode to the Nafion 117 at 160 °C and 1000 kgf cm^{-2} for 10 min. The fabricated electrodes were evaluated in 5 cm^2 single fuel cell. The single cell was fed with ethanol/NaOH solution (2.0 mol L^{-1}/6.0 mol L^{-1}) and 3.0 mL min^{-1} flux at the anode and with pure oxygen in large excess. Fuel and oxygen humidifiers were kept at 100 °C and 90 °C and 1 atm and 2 atm absolute pressures, respectively. The single fuel cell was stabilized for 200 min at constant measuring temperature. Polarization curves were measured in duplicate experiments, with estimated error of ~10%, using a potentiostat/galvanostat Autolab PGSTAT 302N. Stability tests were performed and the polarization curves were recorded up to 450 min of measurements.

Results and discussions

The functionalization of the carbon can be studied by thermogravimetric analysis (TGA).

As showed in Fig. 1a, the functionalized carbon (Vulcan-F) displays the characteristic mass loss associated with the decomposition of the superficial functional groups incorporated during the functionalization; whereas no noticeable mass loss is observed for Vulcan up to ~ 700 °C. The TGA curve of Vulcan-F exhibits the first mass loss (~2.5%) in the ~25–100 °C *T*-range, which can be attributed to the loss of adsorbed water [24,30]. This result is in accordance with previous studies that evidenced a more hydrophilic surface for functionalized carbon due to the presence of carboxylic acid groups [30]. Such feature is confirmed by observing the mass losses occurring in the ~170–300 °C (~2.5%) and ~600–730 °C (~2.5%), which are the intervals that occurs the typical mass losses due to the decomposition of carboxylic (~250 °C) and anidrides (~630 °C) groups, respectively [32].

In order to estimate the catalyst loading supported on the carbon during synthesis, TGA measurements were carried out as shown in Fig. 1b and c. It can be seen that all samples exhibit four mass loss events in the ~25–900 °C *T*-range. The first mass loss (*T* ~ 25–100 °C) corresponds to the removal of absorbed water [26,27]. It can be observed that a larger fraction of water is removed from the samples containing nickel (~8%) compared to the unary catalysts (~3%). It was reported that the Ni in binary and ternary Pd-compounds can contain oxy-hydroxy Ni compounds in their composition, which are hydrophilic phases that can adsorb large amounts of water [26,27]. The second mass loss, occurring from ~100 to ~250 °C is also more evident in nickel-based catalysts, whereas no noticeable mass loss is observed for Pd and PdSn samples. The mass loss observed for PdNi and PdNiSn can be assigned to conversion of nickel hydroxide to nickel oxide [26,27]. Carbon was reported to

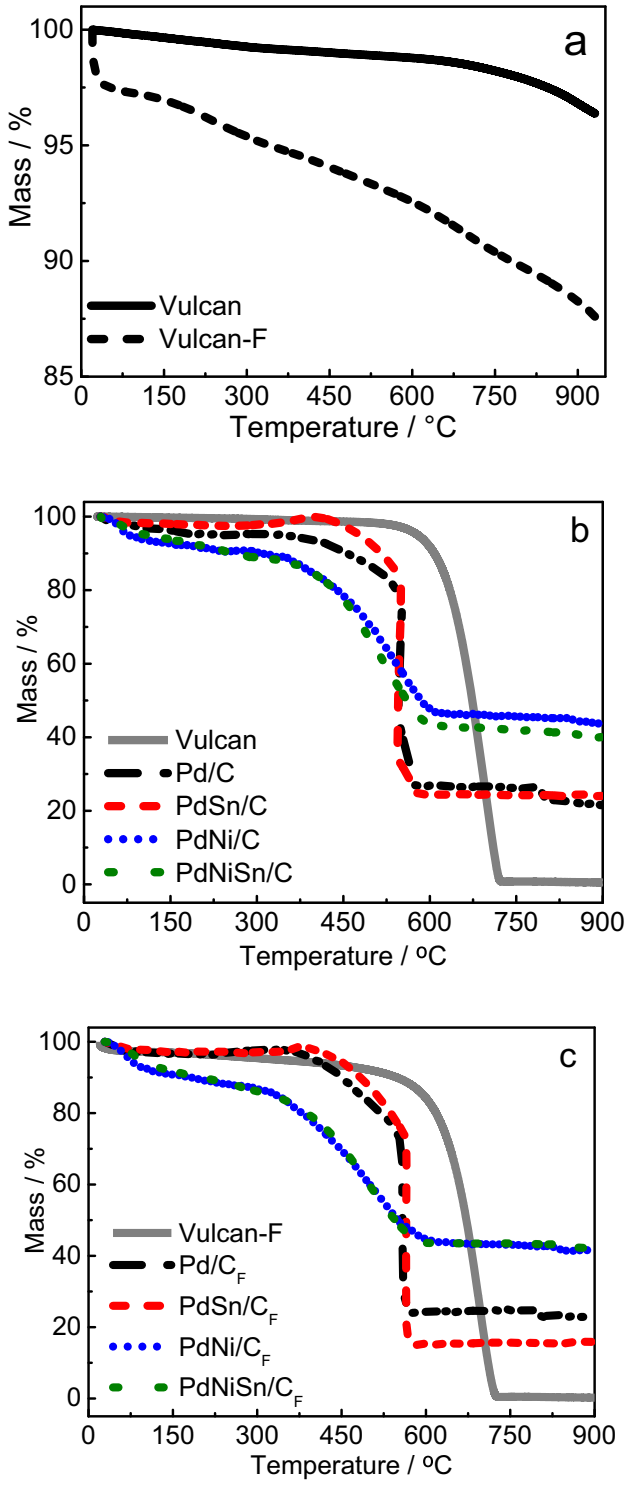

Fig. 1 – Thermogravimetric analysis for Vulcan and Vulcan-F under N_2 flow (a); and for the Pd, PdSn, PdNi, and PdNiSn electrocatalysts supported on non-functionalized (b) and functionalized (c) Vulcan under synthetic air flow.

decompose at ~300 °C reaching a complete oxidation at ~600 °C [26,27]. In Fig. 1, the onset of mass loss is observed at ~350 °C. It is worth noting that in the ~250–350 °C *T*-range the Pd and PdSn catalysts exhibit a mass gain (~1%), which can be ascribed to the oxidation of Pd forming PdO [31]. It can be noted that such behavior of increasing mass in the ~250–350 °C *T*-range is observed for Pd and PdSn catalysts, while PdNi and PdNiSn catalysts exhibited decreasing mass in the entire temperature range. According to previous reports the PdO↔Pd reactions are initiated mainly at the particle surface as identified by transmission electron microscopy (TEM) and TGA measurements [33,34]. In this context, the absence of mass gain due to the oxidation of Pd in the PdNi and PdNiSn is possibly a result of segregated oxide phases on the Pd surface, which inhibit an extensive oxidation to PdO. The similar TGA profiles observed for Pd and PdSn is in agreement with previous reports that indicated a high degree of alloying between Pd and Sn [13]. The forth mass loss occurs at ~800 °C due to thermal decomposition of PdO to Pd [31]. Therefore, the remaining mass at ~900 °C can be used to estimate the catalyst loading supported on carbon, and by using the atomic ratios, the amount of Pd of each catalyst can be estimated.

The catalyst loading estimated from TGA curves at 900 °C (Fig. 1b and c) and the Pd content of each electrocatalyst estimated from the atomic ratios measured by EDX are listed in Table 1.

The measured EDX and RBS atomic ratios of the electrocatalysts are close to the nominal values with deviations within the experimental error (<10%). The catalyst loading for the Pd and PdSn catalysts ranges from ~16 to 24%, whereas the catalyst loading observed for PdNi and PdNiSn are substantially elevated (~40–44%). It is worth noting that the estimated amount of Pd supported on Vulcan during the synthesis of the different catalysts has not exceeded ~25% (Table 1).

It can be inferred from a comparison between the catalyst and Pd loadings that the higher catalyst loading observed for PdNi is possibly a result of segregated nickel oxide/hydroxide phases on the Pd surface [2]. Moreover, both the catalyst and Pd loadings of Pd and PdSn are comparable indicating that the presence of segregated tin oxide on Pd surface is negligible. This result suggests that the higher catalyst loading of PdNiSn (~40%) can be mostly attributed to segregated nickel oxide/hydroxide on Pd [2]. Such features can be better evaluated with XRD analysis.

X-rays diffraction patterns of both functionalized and non-functionalized carbon supported Pd, PdSn, PdNi, and PdNiSn are shown in Fig. 2.

In Fig. 2a and b, it can be observed that the XRD patterns of all electrocatalysts displayed the typical diffraction peaks [(111), (200), (220) and (311) planes] of the Pd fcc structure (JCPDS 46-1043). The XRD patterns of PdNi and PdNiSn (Fig. 2) exhibit the diffraction peaks of oxide phase NiO [(110)], indicating a trend of formation of segregated phases in PdNi-based systems. However, a close inspection of the (111) peak (Fig. 2c and d) reveals a slight displacement to higher angles for PdNi samples indicating that a small fraction of Ni content could be incorporated into the crystalline lattice of Pd. Such high angle displacement was previously observed for PtNi catalysts and was attributed to a contraction of the Pd lattice upon the introduction of the lower atomic radii Ni [28]. The difficulty of forming alloy between Pd and Ni has been reported previously, and the XRD data (Fig. 2) indicate that the impregnation-reduction method in alkaline media used in the catalyst synthesis allowed the partial insertion of metallic nickel in the Pd sample [2].

Table 1 – Nominal atomic ratio, EDX and RBS atomic ratios, catalyst loading, and the estimated Pd content based on the EDX atomic ratio for the prepared electrocatalysts.

Electrocatalyst	Nominal atomic ratio %	EDX atomic ratio %	RBS atomic ratio %	Catalyst loading %	Pd content %
Pd/C	100	–	–	21.5	21.5
Pd/C_F	100	–	–	22.6	22.6
PdSn/C	86:14	82:18	82:18	24.0	19.7
PdSn/C_F	86:14	83:17	86:14	15.9	13.2
PdNi/C	60:40	58:42	60:40	43.8	25.4
PdNi/C_F	60:40	58:42	60:40	41.8	24.2
PdNiSn/C	40:50:10	43:44:13	40:48:12	40.0	17.2
PdNiSn/C_F	40:50:10	42:45:13	38:51:11	42.1	17.7

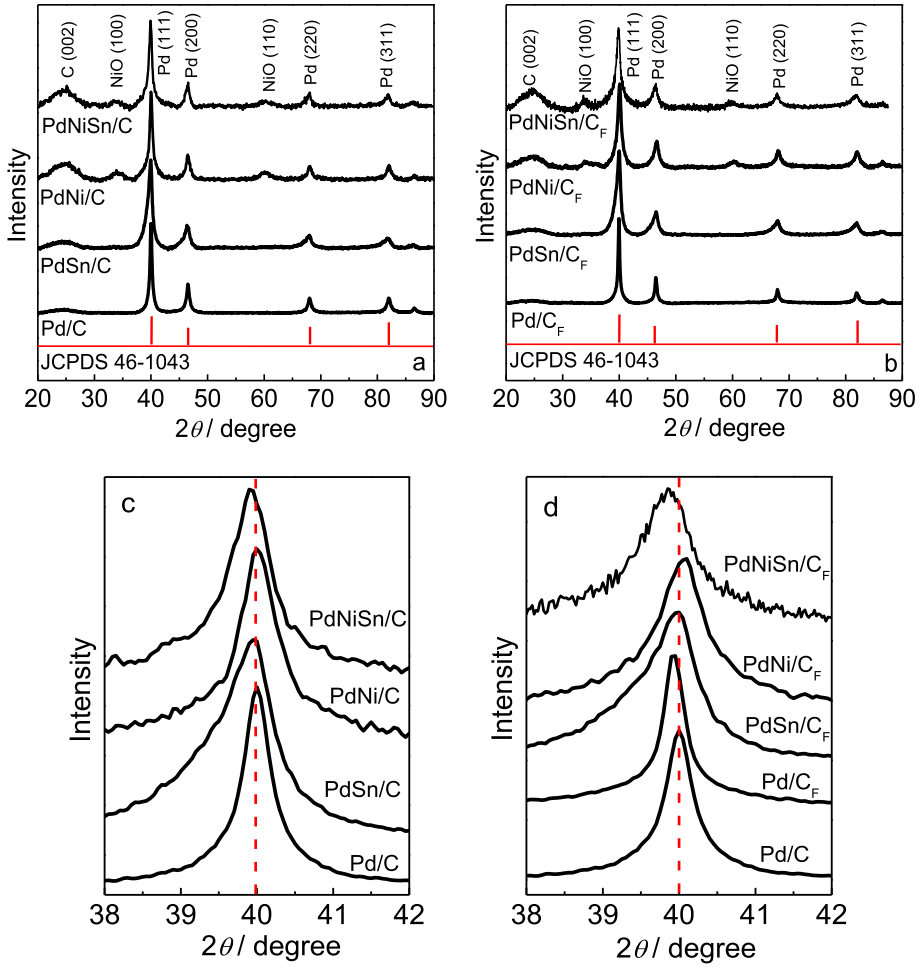

Fig. 2 – XRD patterns of (a) non-functionalized and (b) functionalized carbon supported binary and ternary electrocatalysts. Expanded view of the (111) peak of (c) non-functionalized and (d) functionalized electrocatalysts.

On the other hand, Fig. 2b and c shows that the diffraction peaks of the binary and ternary electrocatalysts PdSn and PdNiSn displaced to lower 2θ values compared to Pd in the following sequence: 2θ ~40.00° (Pd/C) > 39.96° (PdSn/C) ~ 39.96° (PdSn/C_F) > 39.92° (PdNiSn/C) > 39.84° (PdNiSn/C_F). The displacement observed for PdNiSn/C_F (Fig. 2c) is similar to the displacement previously observed for PdSn/C (~0.2°) with respect to Pd/C [13], which can be attributed to the alloy formation between Pd and Sn [13]. An additional feature observed in the XRD plots of PdSn and PdNiSn samples is the skewed shapes of the all the observed peaks (Fig. 2b and d). Such peaks were previously observed for higher amounts of Sn ($Pd_{75}Sn_{25}$/C) in the electrocatalysts, which were prepared with modified polyol method very similar to the one used in this study [13]. The asymmetry of the PdSn and PdNiSn peaks is possibly associated with a distortion of the Pd lattice to a more orthorhombic structure due to the incorporation of Sn [13]. However, it can be observed that the peak asymmetry was observed even for $Pd_{84}Sn_{16}$ (Fig. 2), indicating that impregnation-reduction method carried out in alkaline media could provide alloy formation between Pd and Sn. Previous XRD studies on PdSn based catalysts identified the presence of

additional peaks corresponding to the (101) and (211) reflections of the SnO_2 at 2θ ~34 and 52°, respectively [29]; however, the XRD patterns of Sn and SnO_2 were not observed for the catalysts containing Sn, indicating that the amount of these phases are negligible.

In order to study the distributions and particle sizes of catalyst nanoparticles, representative TEM images alongside with the particle size histograms for the functionalized and non-functionalized electrocatalysts were obtained and shown in Fig. 3.

It can be observed that the average particle sizes ranged from ~5.7 to 12.2 nm indicating that the reduction method with ethylene glycol allowed producing small nanoparticles, in good agreement with previous reports [24]. The functionalized Pd (Fig. 3a and b) and PdSn (Fig. 3c and d) exhibited a higher degree of particle agglomeration, whereas the PdNi (Fig. 3e and f) and PdNiSn (Fig. 3g and h) samples displayed a more uniform particle size distribution.

Table 2 shows the average crystallite and particle sizes as estimated by XRD and TEM, respectively, and the electrochemical active surface area (EASA) estimated by cyclic voltammetry. The particle/crystallite size for Pd (Table 2) is in good agreement with previously reported values [24]. Previous functionalization studies of the carbon support reported either an increase and a decrease of Pd crystallite sizes with respect to the non-modified carbon [23,24]. Accordingly, Table 2 shows that the functionalization of the carbon support resulted in electrocatalysts with smaller particle and crystallite sizes, except for Pd samples in which the opposite was observed. The average crystallite and particle sizes estimated from XRD and TEM, respectively, show a good agreement of the estimated average sizes by both techniques. The different size distributions may arise from several factors, including different percentage compositions, possibly the most critical ones are the ability of the co-catalyst to form alloys with Pd, the possibility of the co-catalyst to form segregated oxide phases, functionalization of the carbon support, and the concentration of the precursors in solution [35].

It can be seen in Table 2 that EASA value for Pd/C is in good agreement with reported data [23,24]. It is worth noting that the EASA is a measure of the Pd active area of each electrocatalyst, the additional area of the incorporated oxide phases is not accounted. This feature indicates that the lower EASA for PdNi is a result of the pronounced coverage of the Pd surface area. PdSn and PdNiSn electrocatalysts displayed higher EASA than the remaining samples; a feature possibly related to the low average crystallite size of PdSn and PdNiSn samples.

Fig. 4 shows typical cyclic voltammograms for the functionalized and non-functionalized Pd-based electrocatalysts in 1 M EtOH and 1 M NaOH solution at ~25 °C. The data obtained in Fig. 4, such as potential onset (E_{onset}), peak potential (E_{peak}) and peak current density (i_{peak}), for the ethanol oxidation are summarized in Table 3.

In Table 3, it can be seen a displacement of the onset potential towards more negative values for PdSn, PdNi, PdNiSn samples supported on functionalized Vulcan when compared to the non-functionalized ones, indicating that the ethanol oxidation is facilitated on such surface. Moreover, except for PdNi, an increase in current density values was identified by CV for functionalized samples with respect to the non-functionalized ones. The current density increase may be attributed to the transport properties conferred to the surface functionalized Vulcan, which contains a higher amount of ion-conducting carboxylic groups [24,30]. Possibly, the functionalization improves removal of ion species from the catalyst surface favoring the continuity of the catalytic reactions. A comparison between the different electrocatalysts, Pd/C_F and $PdSn/C_F$ demonstrate higher values of current density, confirming the effectiveness of Sn as co-electrocatalyst in the ethanol electrooxidation in alkaline medium.

PdNi samples with respect to Pd/C electrocatalyst showed a pronounced decrease in the peak current density and a similar onset potential. According to TEM analysis, the Pd/C and PdNi/C have similar particle-size distributions and average particle sizes indicating that the difference in the catalytic activity between Pd/C and PdNi/C is independent on the particle size. In addition, it was evidenced by XRD a majority presence of segregated oxide-type Ni electrocatalyst, which has no apparent contribution to the catalytic activity of PdNi/C samples [2]. On the other hand, previous studies showed that higher catalytic activity for EOR was achieved for PdNi compounds from low to high Ni concentrations (Pd_1Ni_1, Pd_2Ni_3 and Pd_1Ni_2) with respect to Pd [2,14]. This characteristic indicates that the low activity of PdNi (Fig. 4) samples can be a result of the high coverage of electron-insulating nickel oxide on the Pd surface, as evidenced in Table 2. Nevertheless, the addition of Sn into the PdNi catalysts showed to improve significantly the kinetics of EOR displaying a higher catalytic activity than the observed for PdNi (Fig. 4). The higher catalytic activity of PdNiSn with respect to PdNi can be a result of the oxophilic nature of the PdNiO/OH surface, and to the modified electronic structure of Pd through the incorporation of Sn in the lattice, both of which favors the oxidative desorption of intermediate products and increases the specific catalytic activity.

Fig. 5 shows the long-term stabilities obtained from the maximum current density (i_{peak}) as a function of cycles (~145 min) of the EOR.

No noticeable changes in current density decay with increasing time was observed for the functionalized samples with respect to the samples supported on unmodified carbon. In addition, Pd/C electrocatalysts have presented the highest oxidation activity followed by PdSn/C, PdNiSn/C, and PdNi/C, which is in good accordance with Fig. 4. This characteristic indicates that the Pd, PdSn and PdNiSn catalysts are more resistant to the poisoning by CO-like species. The higher capability in resisting poisoning of intermediates was previously attributed to both the oxophilic Ni species and the transformation between $Ni(OH)_2$ and NiOOH [2]. In Fig. 5, it is shown that the all the functionalized and non-functionalized samples exhibit similar stabilities for measurements above 80^{th} cycle (60 min). Apparently, no appreciable lixiviation of non-noble metals occurs in PdNi-based electrocatalysts, possibly due to the segregated nickel oxide phase, which justify low values of ethanol oxidation current densities.

Fig. 6 shows the polarization and power density curves of ADEFC (alkaline direct ethanol fuel cell) operating with anodes based on Pd, PdSn, PdNi, and PdNiSn supported in both functionalized and non-functionalized Vulcan carbon.

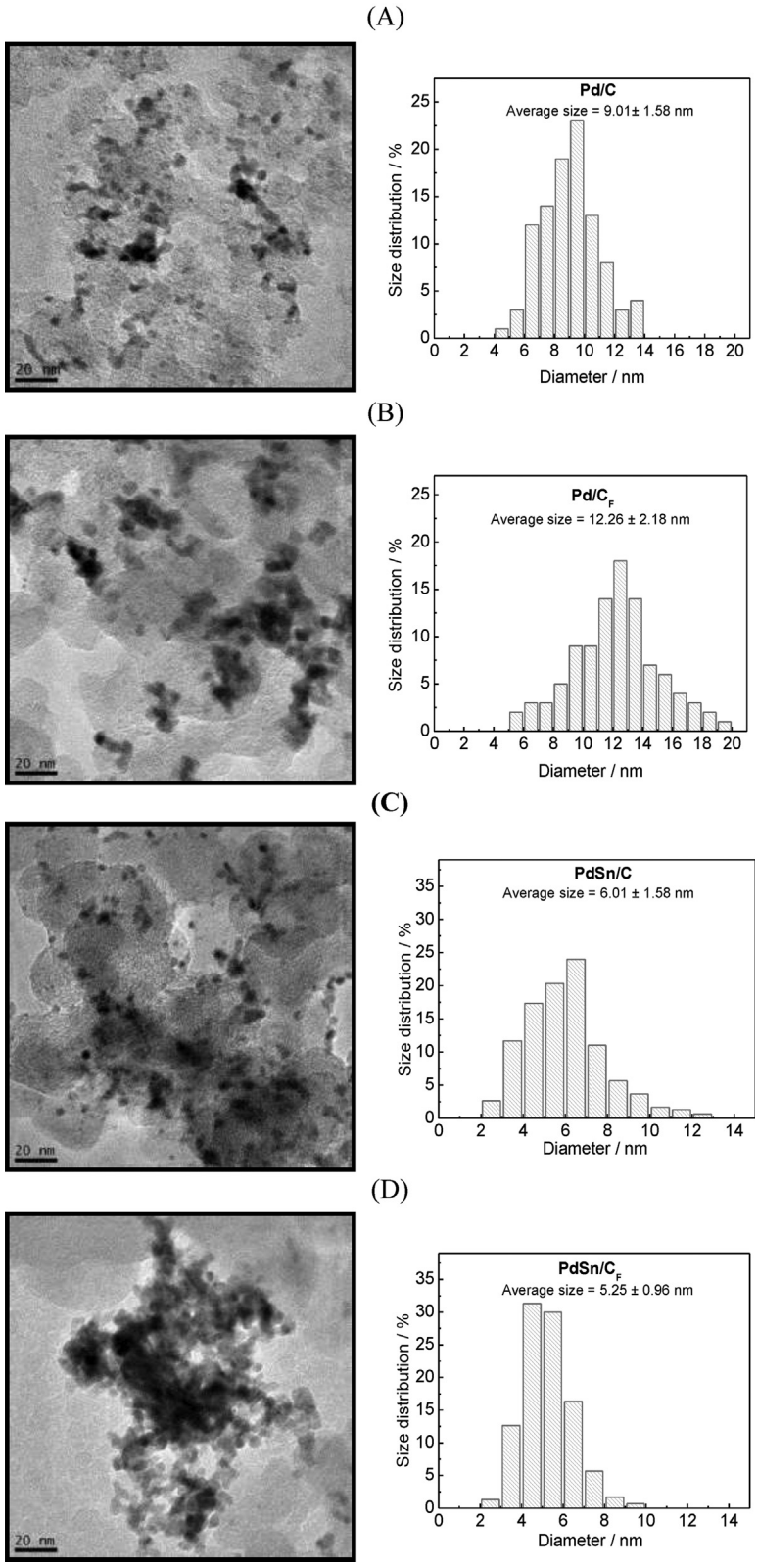

Fig. 3 – Representative TEM images of the functionalized and non-functionalized carbon-based Pd (A and B), PdSn (C and D), PdNi (E and F) and PdNiSn (G and H) alongside with the respective histograms displaying the particle size distribution.

The polarization (*I*–*V*) curves evidenced typical features of ADEFC: *i*) a large drop of the open circuit voltage (OCV) with respect to the theoretical equilibrium potential for ethanol electrooxidation (E_{eq} ~ 1.145 V/T = 25 °C) and *ii*) a large polarization loss at low current densities due to activation polarization [1,2]. The OCV drop is usually attributed to the

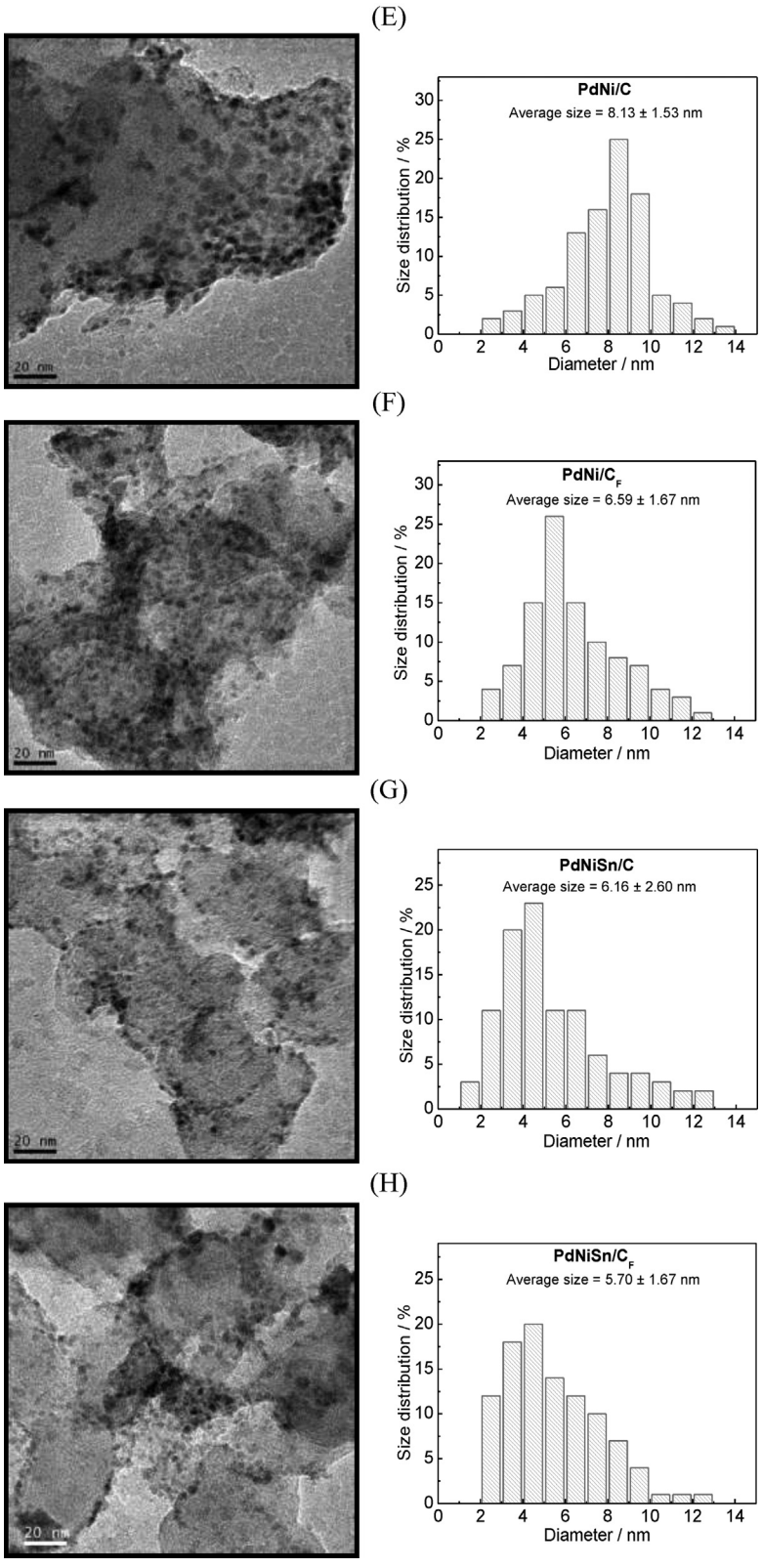

Fig. 3 – (*continued*).

crossover of ethanol molecules from the anode to the cathode due to the high ethanol permeability characteristic of Nafion membranes, whereas the activation polarization is attributed to the sluggish ethanol oxidation reaction [1]. Thus, taking into account that the studied fuel cells have nominally identical membranes and cathodes, the differences observed in

Table 2 – Average TEM and XRD particle and crystallite sizes, and the electrochemical active surface area for the prepared electrocatalysts.

Electrocatalyst	Crystallite size DRX (nm)	Particle size TEM (nm)	EASA ($m^2\ g^{-1}$)
Pd/C	12.94	9.01 ± 1.58	8.23
Pd/C_F	14.43	12.26 ± 2.18	3.82
PdSn/C	6.05	6.01 ± 1.58	15.73
$PdSn/C_F$	5.47	5.25 ± 0.96	11.60
PdNi/C	10.59	8.13 ± 1.53	1.33
$PdNi/C_F$	7.26	6.59 ± 1.67	3.02
PdNiSn/C	7.07	6.16 ± 2.60	9.45
$PdNiSn/C_F$	6.32	5.70 ± 1.67	5.10

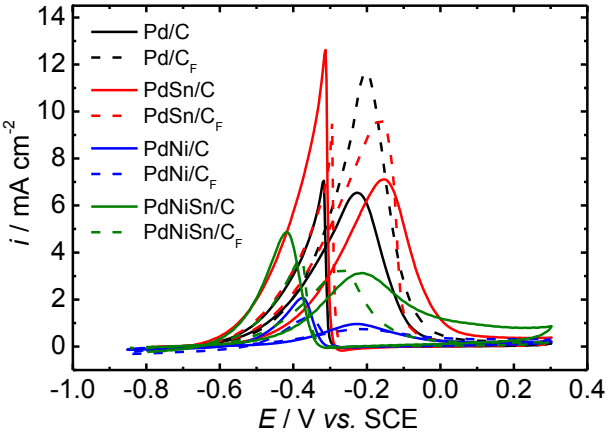

Fig. 4 – Cyclic voltammograms for the electrooxidation of ethanol on Pd based electrodes in 1.0 M NaOH and 1.0 M EtOH with a sweep rate of 50 mV s^{-1}.

Table 3 – Onset potential (E_{onset}), peak current density (i_{peak}) and peak potential (E_{peak}) for the EOR on the Pd based electrocatalysts.

Catalyst	E_{onset} (V)	i_{peak} (mA cm^{-2})	E_{peak} (V)
Pd/C	−0.45	6.54	−0.22
Pd/C_F	−0.43	11.69	−0.20
PdSn/C	−0.39	7.12	−0.15
$PdSn/C_F$	−0.43	9.69	−0.17
PdNi/C	−0.41	0.96	−0.23
$PdNi/C_F$	−0.45	0.74	−0.22
PdNiSn/C	−0.42	3.14	−0.21
$PdNiSn/C_F$	−0.48	3.27	−0.27

the polarization curves, markedly at low current densities, are essentially related to the properties of the investigated anodes [2].

Table 4 shows the specific resistance (*R*), the open circuit voltage (OCV) and the maximum power density (p_{max}) for the prepared electrocatalysts. The OCV values and maximum power density are obtained directly by the polarization and power density curves, respectively. The specific ohmic resistances are mainly associated with the ion transport resistances of the catalyst layer and of the Nafion membrane [25]. The *R* was estimated by fitting the linear portion of the *I*–*V* curves in Fig. 6. It can be observed, that the *R*-values for

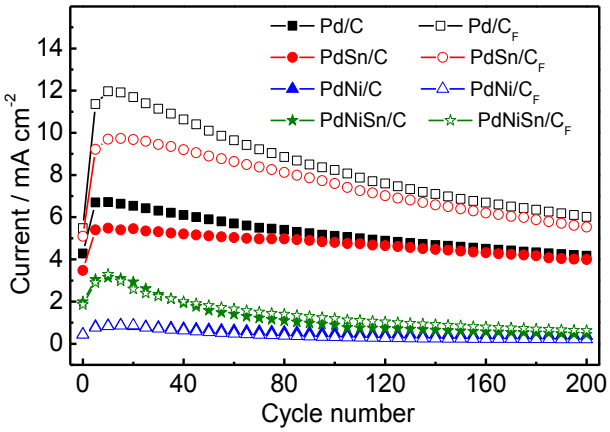

Fig. 5 – Long-term stabilities obtained from the maximum current density (i_{peak}) as a function of cycles (~145 min) of the EOR for the catalysts.

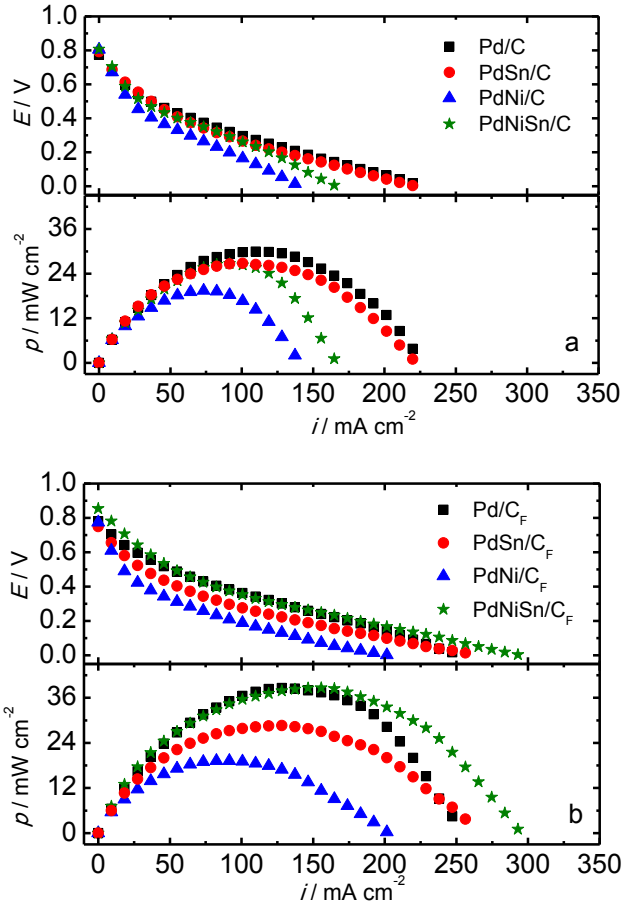

Fig. 6 – Polarization (*I*–*V*) curves and power density curves for non-functionalized (a) and functionalized (b) Pd/C and Pd-based binary and ternary electrocatalysts. The cell was fed with EtOH/NaOH (2 M/6 M) solution with 3 mL min^{-1} ethanol flux at *T* ~ 100 °C.

the functionalized electrocatalysts are lower than the non-functionalized ones. This finding can be a result of the ion transport properties conferred to the Vulcan upon surface functionalization with carboxylic groups.

Table 4 – Specific resistance (R), open circuit voltage (OCV) and maximum power density (p_{max}) for the prepared electrocatalysts.

Catalysts	R (Ω cm^2)	OCV (mV)	p_{max} (mW cm^{-2})
Pd/C	2.43	774	30.1
Pd/C$_F$	2.24	779	38.4
PdSn/C	2.28	793	27.2
PdSn/C$_F$	1.81	751	28.6
PdNi/C	3.58	804	19.8
PdNi/C$_F$	2.16	774	19.4
PdNiSn/C	2.99	807	27.1
PdNiSn/C$_F$	1.88	858	38.8

It can be inferred from Table 4 that the open circuit voltage (OCV) of the ADEFC using PdSn/C$_F$ (~751 mV) decreases with respect to Pd/C$_F$ (~779 mV); the OCV of Pd/C$_F$ and PdNi/C$_F$ (~774 mV) are similar; whereas a significant increase of the OCV is observed for PdNiSn/C$_F$ electrocatalysts (~858 mV). The higher OCV for the fuel cell with PdNiSn/C$_F$ and PdNiSn/C represents a gain of ~79 mV and ~33 mV in the ADEFC performance with respect to Pd/C$_F$ and Pd/C, respectively. No systematic relationship can be observed for the functionalization of the carbon support and the OCV values. For the non-functionalized samples the OCV values are similar for PdNi/C and PdNiSn/C exhibits the highest OCV values. It is worth noting that PdNi and PdNiSn exhibited a more uniform distribution of nanoparticles (Fig. 3).

The OCV values are mainly related to the ethanol crossover. Thus, the reduction of fuel crossover can be understood considering the specific surface area of each catalyst and distribution of electrocatalyst particles in the carbon support. The TEM analysis showed that Pd and PdSn exhibited a higher degree of agglomeration in comparison with the PdNi and PdNiSn catalysts (Fig. 3). Another factor that can contribute to the lower ethanol crossover in anodes containing PdNi and PdNiSn is the presence of oxide phase in the catalysts. Previous DEFC fuel cell tests evidenced a suppression of the ethanol crossover in Nafion electrolytes by the addition of a hydroxyl-rich oxide phase [18]. The improved dispersion of the PdNiSn catalyst increases the interface between the fuel and the catalyst surface, thereby increasing the number of adsorption sites for ethanol, which inhibits the ethanol diffusion towards the electrolyte.

A general feature that can be observed for all electrocatalysts is that the maximum power density has a correspondence with the OCV values and the specific resistance, indicating that higher ADEFC performances can be achieved by only changing the electrode microstructural features such as, support functionalization, particle distribution and specific surface area. This finding has been previously observed for DEFC measurements, which showed that a pronounced increase of the DEFC performance was obtained by solely decreasing the ethanol crossover from the electrolyte by using composite membranes [18]. It is worth emphasizing that the increase of OCV and the reduction of the specific resistance were the main effects of increasing the ADEFC performance of Fig. 6; a feature that has been bypassed in several studies of electrocatalysts on ADEFC. The second parameter observed to increase the ADEFC performance is the catalytic activity. The study of the ethanol electrooxidation for Pd, PdSn and PdNi shown in Fig. 4 reflected in the ADEFC performance. In Fig. 4, Pd and PdSn exhibited similar peak current densities, PdNi showed the lowest i_{peak} values whereas the PdNiSn displayed intermediary i_{peak} values (Table 3). Similarly, in ADEFC tests, the *p*-values for Pd/C (p_{max} ~ 30.1 mW cm^{-2}) and PdSn/C (p_{max} ~ 27.2 mW cm^{-2}) are similar, whereas an inferior p_{max} is observed for the PdNi/C (p_{max} ~ 19.8 mW cm^{-2}). This relationship can be also observed for the functionalized samples. However, the PdNiSn/C (p_{max} ~ 27.1 mW cm^{-2}) and PdNiSn/C$_F$ (p_{max} ~ 38.8 mW cm^{-2}) exhibited an unexpected high performance in ADEFC, which is attributed to the electrode texture rather than the catalytic activity.

Although a large EASA was obtained for Pd and PdSn catalysts (Table 2), such large EASA values are calculated based on the oxidation of Pd to PdO in which the oxygen diffusion towards the catalyst layer may have access to such agglomerated structure. Possibly, the surface area for the ethanol adsorption on the agglomerated Pd and PdSn is reduced.

Fig. 7 shows the maximum power density for the electrocatalysts as a function of time.

It can be noted that the performance of Pd samples decreases more pronouncedly compared to the other catalysts, in agreement with the electrochemical data, indicating that the loss of performance can be mainly attributed to the electrodes performance (both anode and cathode). However, although an accentuated reduction of the current density values are observed in CV tests (0 < t < 145 min), the ADEFC performance decays more pronouncedly only for t > 250 min. This feature can be associated with the longer period (~100 min) that is required to reach the steady state in ADEFC measurements compared to CV tests (~60 min). The long-term ADEFC tests indicate that although the electrode's texture is intimately associated with the ADEFC performance, the loss of power density depends mostly on the catalytic activity of the electrocatalysts. This finding is in good agreement with previous ADEFC stability tests of Pd, which revealed that the main parameters involved with the fuel cell performance loss were associated with changes of the particle size and distribution as well as the changes of nanoparticle morphology [13,17].

The highest power density observed for PdSn/C and PdNiSn/C$_F$ indicates that a tradeoff of several parameters improves the ADEFC performance. Among binary and ternary

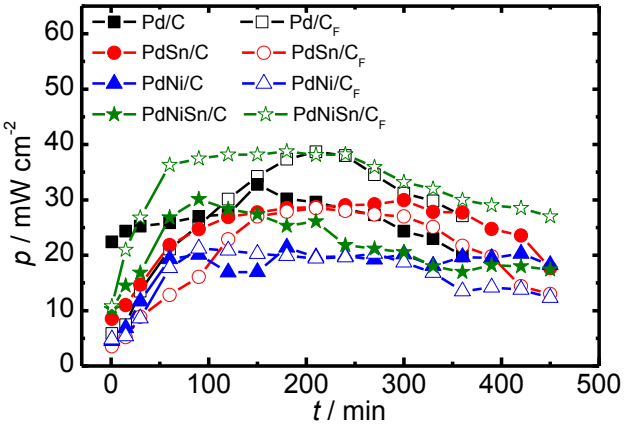

Fig. 7 – Maximum power density of ADEFC for the electrocatalysts as a function of time.

electrocatalysts, PdSn-based electrocatalysts, including PdNiSn/C, showed better performance than PdNi/C, which might be related to lower alloying degree of Ni in PdNi/C electrocatalysts and/or and extensive surface coverage of Pd. However, the PdNiSn/C_F exhibited a more pronounced increase of the maximum power density (p_{max} ~ 38.2 mW cm^{-2}) with respect to the other catalysts (p_{max} ~ 20.0–34.1 mW cm^{-2}). PdNiSn/C_F has a catalytic activity superior than PdNi, a uniform distribution of nanoparticles, and a lower ohmic resistance. All these features contributed to enhance the ADEFC performance and stability. It is interesting to point out that using non-functionalized carbon, the PdSn/C displayed a similar performance than PdNiSn/C (Fig. 6a) indicating that the higher catalytic activity of PdSn was the predominant role in enhancing the ADEFC performance.

Conclusion

The comparison of different Pd-based electrocatalysts as ADEFC anodes allowed identifying the main parameters, such as particle distribution, functionalization of the carbon support, surface active area and catalytic activity, which were responsible for the enhancement of ADEFC performance. The high specific surface area and homogeneity in the catalyst distribution of PdNiSn contributed to reduce the ethanol crossover and increase the open circuit voltage. The specific resistance of ADEFC using catalysts supported on functionalized Vulcan was lower than the ones on unmodified Vulcan, indicating that an improved interface exists among the catalyst/carbon/electrolyte at the catalyst layer. The study of the physical and physicochemical properties of PdNiSn catalysts which indicated that an optimized ADEFC performance is achieved by using anodes with high kinetics for EOR and reduced particle sizes and uniform distributions.

Acknowledgment

Thanks are due to the Brazilian Funding Agencies (PRH-ANP 38, CAPES, CNPQ, 2013/50151-5 and 2014/08097-4 FAPESP) and CNEN.

REFERENCES

[1] Antolini E, Gonzalez ER. Alkaline direct alcohol fuel cells. J Power Sources 2010;195:3431.
[2] Shen SY, Zhao TS, Xu JB, Li YS. Synthesis of PdNi catalysts for the oxidation of ethanol in alkaline direct ethanol fuel cells. J Power Sources 2010;195:1001.
[3] Xu C, Shen P, Liu Y. Ethanol electrooxidation on Pt/C and Pd/C catalysts promoted with oxide. J Power Sources 2007;164:527.
[4] Bianchini C, Bambagioni V, Filippi J, Marchionni A, Vizza F, Bert P, et al. Selective oxidation of ethanol to acetic acid in highly efficient polymer electrolyte membrane-direct ethanol fuel cells. Electrochem Commun 2009;11:1077.
[5] Zhou ZY, Wang QA, Lin JL, Tian N, Sun SG. In situ FTIR spectroscopic studies of electrooxidation of ethanol on Pd electrode in alkaline media. Electrochim Acta 2010;55:7995.
[6] Mann J, Yao N, Bocarsly AB. Characterization and analysis of new catalysts for a direct ethanol fuel cell. Langmuir 2006;22:10432.
[7] Liang ZX, Zhao TS, Xu JB, Zhu LD. Mechanism study of the ethanol oxidation reaction on palladium in alkaline media. Electrochim Acta 2009;54:2203.
[8] Xu C, Wang H, Shen PK, Jiang SP. Highly ordered Pd nanowire arrays as effective electrocatalysts for ethanol oxidation in direct alcohol fuel cells. Adv Mater 2007;19:4256–9.
[9] Tsui L-K, Zafferoni C, Lavacchi A, Innocenti M, Vizza F, Zangari G. Electrocatalytic activity and operational stability of electrodeposited Pd-Co films towards ethanol oxidation in alkaline electrolytes. J Power Sources 2015;293:815–22.
[10] del Rosario JAD, Ocon JD, Jeon H, Yi Y, Lee JK, Lee J. Enhancing role of nickel in the nickel–palladium bilayer for electrocatalytic oxidation of ethanol in alkaline media. J Phys Chem C 2014;118:22473–8.
[11] Jurzinsky T, Bär R, Cremers C, Tübke J, Elsner P. Highly active carbon supported palladium-rhodium PdXRh/C catalysts for methanol electrooxidation in alkaline media and their performance in anion exchange direct methanol fuel cells (AEM-DMFCs). Electrochim Acta 2015;176:1191–201.
[12] Carrera-Cerritos R, Fuentes-Ramírez R, Cuevas-Muniz FM, Ledesma-García J, Arriaga LG. Performance and stability of Pd nanostructures in an alkaline direct ethanol fuel cell. J Power Sources 2014;269:370.
[13] Du W, Mackenzie KE, Milano DF, Deskins NA, Su D, Teng X. Palladium–tin alloyed catalysts for the ethanol oxidation reaction in an alkaline medium. ACS Catal 2012;2:287.
[14] Dutta A, Datta J. Energy efficient role of Ni/NiO in PdNi nano catalyst used in alkaline DEFC. J Mater Chem A 2014;2:3237.
[15] da Silva SG, Assumpção MHMT, Silva JCM, De Souza RFB, Spinacé EV, Neto AO, et al. PdSn/C electrocatalysts with different atomic ratios for ethanol electro-oxidation in alkaline media. Int J Electrochem Sci 2014;9:5416.
[16] Li YS, He YL, Yang WW. Performance characteristics of air-breathing anion-exchange membrane direct ethanol fuel cells. Int J Hydrogen Energy 2013;38:13427.
[17] Li YS, Zhao TS, Liang ZX. Performance of alkaline electrolyte-membrane-based direct ethanol fuel cells. J Power Sources 2009;187:387.
[18] Matos BR, Isidoro RA, Santiago EI, Fonseca FC. Performance enhancement of direct ethanol fuel cell using Nafion composites with high volume fraction of titania. J Power Sources 2014;268:706.
[19] Xu CW, Shen PK. Novel Pt/CeO_2/C catalysts for electrooxidation of alcohols in alkaline media. Chem Commun 2004:2238.
[20] West AR. Solid state chemistry and its applications. New York: Wiley; 1984.
[21] Matos BR, Isidoro RA, Santiago EI, Tavares AC, Ferlauto AS, Muccillo R, et al. Nafion–titanate nanotubes composites prepared by in situ crystallization and casting for direct ethanol fuel cells. Int J Hydrogen Energy 2015;40:1859.
[22] Matos BR, Andrade CA, Santiago EI, Fonseca FC. Proton conductivity of perfluorosulfonate ionomers at high temperature and high relative humidity. Appl Phys Lett 2014;104:091904.
[23] Cao J, Song L, Tang J, Xu J, Wang W, Chen Z. Enhanced activity of Pd nanoparticles supported on Vulcan XC72R carbon pretreated via a modified Hummers method for formic acid electrooxidation. Appl Surf Sci 2013;74:138.
[24] Kumar SMS, Herrero JS, Irusta S, Scott K. The effect of pretreatment of Vulcan XC-72R carbon on morphology and electrochemical oxygen reduction kinetics of supported Pd nano-particle in acidic electrolyte. J Electroanal Chem 2010;647:211.
[25] Adjemian KT, Dominey R, Krishnan L, Ota H, Majsztrik PW, Zhang T, et al. Function and characterization of metal

oxide–nafion composite membranes for elevated-temperature H_2/O_2 PEM fuel cells. Chem Mater 2006;18:2238.
[26] Freitas MBJG. Nickel hydroxide powder for $NiO{\cdot}OH/Ni(OH)_2$ electrodes of the alkaline batteries. J Power Sources 2001;93:163.
[27] Mani B, de Neufville JP. Dehydration of chemically and electrochemically impregnated (CI and EI) nickel hydroxide electrodes. J Electrochem Soc 1988;135:800.
[28] Park K-W, Choi J-H, Kwon B-K, Lee S-A, Sung Y-E. Chemical and electronic effects of Ni in Pt/Ni and Pt/Ru/Ni alloy nanoparticles in methanol electrooxidation. J Phys Chem B 2002;106:1869.
[29] Zhu F, Wang M, He Y, Ma G, Zhang Z, Wang X. A comparative study of elemental additives (Ni, Co and Ag) on electrocatalytic activity improvement of PdSn-based catalysts for ethanol and formic acid electro-oxidation. Electrochim Acta 2014;148:291.
[30] Boehm HP. Some aspects of the surface chemistry of carbon blacks and other carbons. Carbon 1994;32:759.
[31] Baylet A, Marecot P, Duprez D, Castellazzi P, Groppi G, Forzatti P. In situ Raman and in situ XRD analysis of PdO reduction and Pd° oxidation supported on γ-Al_2O_3 catalyst under different atmospheres. Phys Chem Chem Phys 2011;13:4607.
[32] Kangasniemi KH, Condit DA, Jarvi TD. Characterization of vulcan electrochemically oxidized under simulated PEM fuel cell conditions. J Electrochem Soc 2004;151:E125.
[33] Datye AK, Bravo J, Nelson TR, Atanasova P, Lyubovsky M, Pfefferle L. Catalyst microstructure and methane oxidation reactivity during the $Pd \leftrightarrow PdO$ transformation on alumina supports. Appl Catal A General 2000;198:179–96.
[34] Farrauto RJ, Hobson MC, Kennelly T, Waterman EM. Catalytic chemistry of supported palladium for combustion of methane. Appl Catal A General 1992;81:227–37.
[35] Silva EL, Vega MRO, Correa PS, Cuña A, Tancredi N, Malfatti CF. Influence of activated carbon porous texture on catalyst activity for ethanol electro-oxidation. Int J Hydrogen Energy 2014;39:14760.